*J. Fluid Mech.* (1976), *vol.* 77, *part* 4, *pp.* 825–842
*Printed in Great Britain*



# On the separation of air flow over water waves

By M. L. BANNER AND W. K. MELVILLE

Department of Theoretical and Applied Mechanics, School of Mathematics, University of New South Wales, Kensington, New South Wales, Australia 2033

(Received 20 February 1976 and in revised form 3 June 1976)

Conditions leading to the onset of air-flow separation over a mobile air–water interface are discussed. It is argued that, in a frame of reference in which the interfacial boundary assumes a steady shape, the occurrence of separation requires a stagnation point on the interface. In the case of air blowing over water waves, this corresponds to the onset of wave breaking. These arguments are strongly supported by flow visualization and pressure measurements carried out in a laboratory wind-wave flume. Furthermore, the pressure measurements show a greatly enhanced interfacial shear stress for a breaking wave compared with that over an unbroken wave of the same wavelength. The implications of these findings for wind-wave generation are discussed.

## 1. Introduction

The dynamics of the air–sea interface have received much attention in recent years, especially mechanisms involved in wind-wave generation. A valuable account of the current status of our empirical and theoretical understanding of this complex problem was recently published by Barnett & Kenyon (1975). From their survey, it is very clear that our present knowledge is still insufficient to construct a satisfactory theory for most phases of air–sea interaction, particularly wind-wave generation as it occurs in the open ocean.

One of the earlier mechanisms proposed was the 'sheltering hypothesis' of Jeffreys (1924, 1925). According to this model, air flowing over a wave separates somewhere on the downwind side of the crest, reattaching on the upwind face of the next crest. This would cause a pressure asymmetry with respect to the wave crest resulting in wave growth. Laboratory experiments conducted over solid waves in wind tunnels (Motzfeld 1937; Stanton, Marshall & Houghton 1932) indicated pressure forces too small for the 'sheltering' mechanism to be an effective one. However, as pointed out by Ursell (1956), the laboratory measurements over solid waves were neither consistent among themselves nor were they entirely relevant to the wind-wave problem. In fact, Barnett & Kenyon (1975) surmise (p. 671) that "Jeffreys' theory may yet emerge as being important since more recent theories (though not completely evaluated yet) based on perturbation techniques have not yielded the major growth mechanism for wind waves. It is still not known, though, whether or not air flow separation does in fact occur over wind waves."

Owing to the observational difficulties associated with defining the air-flow structure near a moving surface wave, direct studies of this problem have not been forthcoming. However, from time to time the presence of air-flow separation has been inferred in isolated laboratory wind-wave studies, e.g. Chang, Plate & Hidy (1971) and Wu (1969). Although lacking direct evidence, Wu (1969) suggested from his results in a wind-wave tank that air-flow separation occurs over waves having a phase velocity less than the shear velocity. He arrived at this criterion indirectly, however, and its validity remains to be verified.

In this paper, we explore both experimentally and analytically the occurrence of air-flow separation over a simple gravity surface wave. A discussion of the features of separation appropriate to the present context is followed by arguments that air flowing over simple water waves should be less prone to separation than air flow over solid boundaries, including wavy walls. Indeed, if the usual kinematic and dynamic boundary conditions are satisfied, air flow should not separate from the surface of a simple gravity surface wave. On the other hand, the onset of wave breaking is sufficient to ensure the existence of air-flow separation. The physical and analytic arguments are supported with direct evidence from flow-visualization studies and pressure measurements made in a laboratory wind-wave flume in which the wave profile was held stationary against a flowing stream. In addition, a momentum integral method has been used to compare the drag over a nominally plane flowing water surface, over an unbroken wave and over a broken wave for a restricted range of flow parameters.

On account of the widespread occurrence of small-scale breaking waves in the ocean, our results stress the need to include the effects of air-flow separation in order to understand and model realistically many aspects of air–sea interaction. Of particular oceanographic interest is the common situation where wind-generated small-scale breaking waves are distributed over an underlying larger-scale wave motion. The sea slick experiments of Barger *et al.* (1970), in which the capillary and small-scale breaking waves were suppressed, suggest strongly the role of these scales in coupling the wind to the larger scales of wave motion (wavelengths up to 10 m in their study). However, Hasselmann (1971) concluded that even upon breaking the small-scale waves do not directly transfer significant momentum and energy to the large-scale waves. The work reported here offers a resolution of this dilemma.

## 2. The onset of air-flow separation

While flow separation is an unsteady phenomenon when associated with turbulent boundary layers, its basic features may be described by a quasi-steady model. Classical flow separation from a rigid stationary wall involves the dynamical effects of viscous and pressure forces under the kinematic constraint of the no-slip boundary condition. Separation usually results from an adverse pressure gradient decelerating the flow to the point where the viscous sublayer flow is brought to rest locally. In order to satisfy mass conservation, the velocity convergence parallel to the wall must be accompanied by an acceleration of the fluid away from the wall, causing a reverse flow in the neighbourhood of the boundary.

Associated with the point of separation is a point of zero shear stress at the boundary ($[\partial u/\partial z]_{z=0} = 0$), which is often used to define the separation point (but see Batchelor 1967, p. 328). In the classical case the kinematic boundary condition is invariant (i.e. all boundary points are potential stagnation points) and the point of onset of separation is dictated more by the dynamics.

In contrast, the kinematic boundary condition for mobile interfaces assumes a more important role. In the following discussion we restrict our attention to moving interface configurations which can be rendered stationary under a suitable uniform translation of the observer. It is then apparent that in this *steady system* the onset of separation as defined above requires the existence of a stagnation point on the boundary. Indeed, concomitant separation of the flows on both sides of the interface is necessary. Experimental configurations which do not satisfactorily model the underlying water motion are unlikely to provide a reliable representation of the behaviour of the air-flow boundary layer over water waves. The experiments of Motzfeld (1937; fixed, solid waves) and Kendall (1970; flexible-membrane wavy wall) are two notable examples. Neither of these experimental configurations was able to model satisfactorily both the kinematic and the dynamic boundary conditions appropriate to water waves. In both cases the dynamic boundary condition is quite different from that at a fluid–fluid interface. Furthermore, in a frame in which the wave profile is steady, every boundary point on the fixed solid waves is a potential stagnation point; from Kendall's (1970) description of the motion of his membrane (p. 262, first paragraph) there were no such stagnation points possible on his wavy membrane. We now examine the flow conditions over a wind-driven water wave to determine under what conditions stagnation points will arise.

For the case of turbulent air flow over a monochromatic surface gravity wave train, it is important to note the existence of viscous sublayers adjacent to the air–water interface. In the water this vortical region, whose depth is very small compared with the wavelength, is known as the wind-drift layer. It has been discussed previously in Banner & Phillips (1974; henceforth referred to as I) and in Phillips & Banner (1974; henceforth referred to as II). Its existence in the present context is of considerable importance as the shear stress in the air-flow sublayer is now determined by the criterion that its value just above the interface should match that just below: the air-flow sublayer dynamics are strongly influenced by the dynamics of the underlying wind-drift layer as well as by the external air flow.

As in I and II, we suppose that, in a reference frame travelling with the unbroken wave profile, the mean motion is steady. We assume that the response time of the wind-drift layer to wind-stress variations is large compared with the wave period. Once the wind-drift layer has been established through viscous action, the further influence of viscosity on the motion in the wind-drift layer may be neglected. To specify the motion, we introduce a locally orthogonal intrinsic co-ordinate system $(s, \eta)$ in which $s$ is the displacement from a suitable origin along the unbroken wavy surface and $\eta = 0$ specifies the surface. Because the depth of the wind-drift layer is very small compared with the wavelength, we assume that the orbital velocity is substantially constant over the depth of the

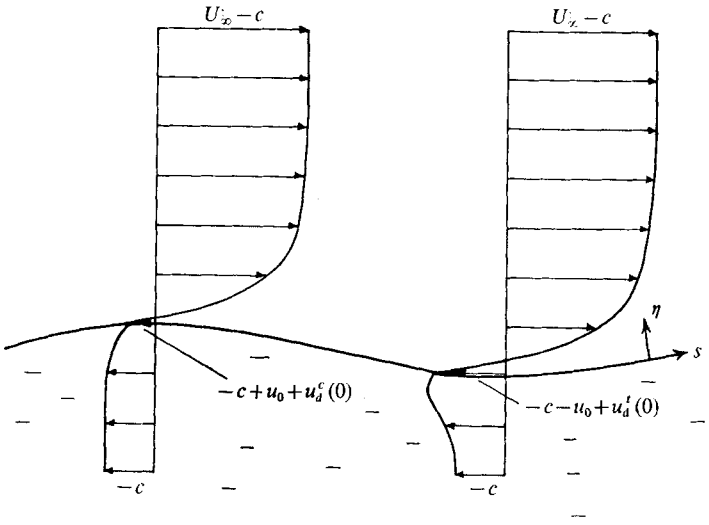


FIGURE 1. Mean velocity profiles at the crest and trough of an unbroken wave. $u_d^c(0)$ and $u_d^t(0)$ are the crest and trough wind-drift velocity increments. $u_0$ is the maximum value of the orbital velocity of the underlying wave motion.

wind-drift layer and that the co-ordinates are locally Cartesian. Within the wind-drift layer, the tangential velocity component is expressible as

$$u = U(\epsilon s) + u_d(\epsilon s, \eta),$$

where $U$ is the irrotational contribution from the orbital velocity and the (horizontal) frame velocity and $u_d$ is the wind-drift velocity increment parallel to the surface (see figure 1). The ratio $\epsilon^{-1}$ of the scales of variation of the velocity in the $s$ direction and in the $\eta$ direction is the ratio of the wavelength to the depth of the wind-drift layer, so that $\epsilon \ll 1$. By continuity, the normal component of the velocity field in the wind-drift layer is

$$v = -\epsilon\eta U'(\epsilon s) + v_d(\epsilon s, \eta)$$

since $v$ and $v_d$ vanish at $\eta = 0$.

In I and II the distribution of wind drift was calculated using the boundary-layer model described above. It was shown there that a stagnation point was possible (at the crest) if $(c-u_0)^2 = q_0(2c-q_0)$. In this equation, $q_0 = (u_d^2+v_d^2)^{\frac{1}{2}}|_{\eta=0}$ is the wind drift where the bounding streamline of the irrotational motion (just below the wind-drift layer) crosses its mean level. It was also shown in I that this incipient breaking condition occurred for wave heights well below the limiting Stokes wave heights for sufficiently large values of $q_0/c$. The same boundary-layer approximation is used here to calculate the shear stress in the wind-drift layer just below the interface. As discussed below, this will influence directly the onset of air-flow separation.

Since $U$ is irrotational, the vorticity field in the wind-drift layer expressed in the orthogonal $s$, $\eta$ co-ordinates in a two-dimensional motion can be shown (Longuet-Higgins 1960, p. 294) to be

$$\omega = (-\partial u_d/\partial\eta)\{1+O(\epsilon)\} \simeq -\partial u_d/\partial\eta.$$

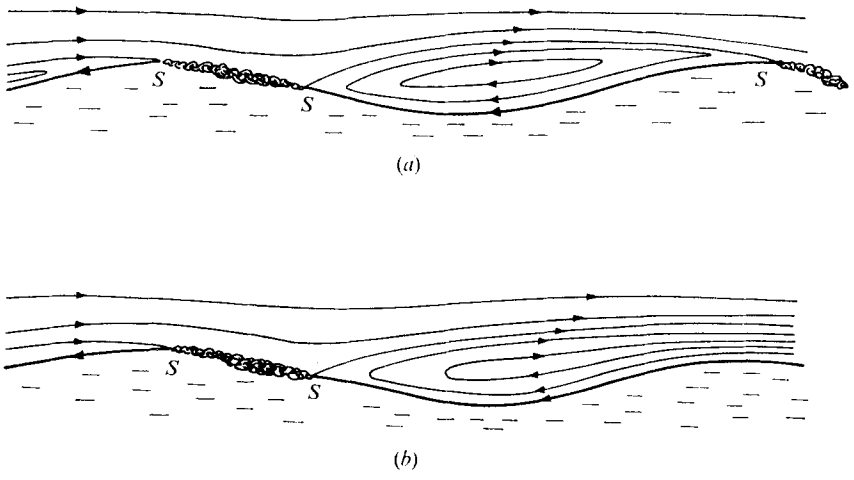


FIGURE 2. Conjectured mean streamlines for the air flow over a broken wave if the downwind wave is (*a*) broken and (*b*) unbroken. The points marked *S* are stagnation points.

Also, to the lowest order in $\epsilon$, the shear stress in the wind-drift layer just below the interface is given by

$$\mu_w[\partial u_d/\partial\eta]_{\eta=0-},$$

where $\mu_w$ is the dynamic viscosity of water. The vorticity balance equation appropriate to the model based on the wind-drift layer assumed above is

$$u\partial\omega/\partial s + v\partial\omega/\partial\eta = 0.$$

As $\eta \to 0$ from below, $v \to 0$ and $u \to u(0-) = u(0)$. Then, to lowest order in $\epsilon$, the vorticity balance equation yields the following result, which holds immediately below the water surface:

$$u(0)\frac{\partial}{\partial s}\left[\frac{\partial u_d}{\partial\eta}(0-)\right] = 0,$$

i.e. the shear in the wind-drift layer immediately below the water surface is constant provided a stagnation point does not occur anywhere along the profile. In this case, since $\mu_a \partial u(0+)/\partial\eta = \mu_w \partial u_d(0-)/\partial\eta$ must hold, we see that

$$\partial u(0+)/\partial\eta \gg \partial u_d(0-)/\partial\eta$$

as $\mu_w/\mu_a = O(10^2)$ ($\mu_a$ is the dynamic viscosity of air). Thus the shear-stress matching to the wind-drift layer maintains a strong velocity gradient in the air-flow viscous sublayer at the boundary, thereby enhancing the stability against air-flow separation for then $\partial u(0+)/\partial\eta$ cannot vanish.

It is noteworthy that the alternative condition $u(0) = 0$ corresponds to incipient breaking of the wave. On physical grounds, wave breaking will lead to a serious modification of the wind-drift layer ahead of the crest; in particular $\partial u_d(0-)/\partial\eta$ will almost certainly suffer a strong discontinuity there. In principle, this is the only configuration which is capable of giving rise to air-flow separation as defined above. We see that the necessary stagnation point and disruption to the stress continuity are present for the breaking wave (as well as an ambient

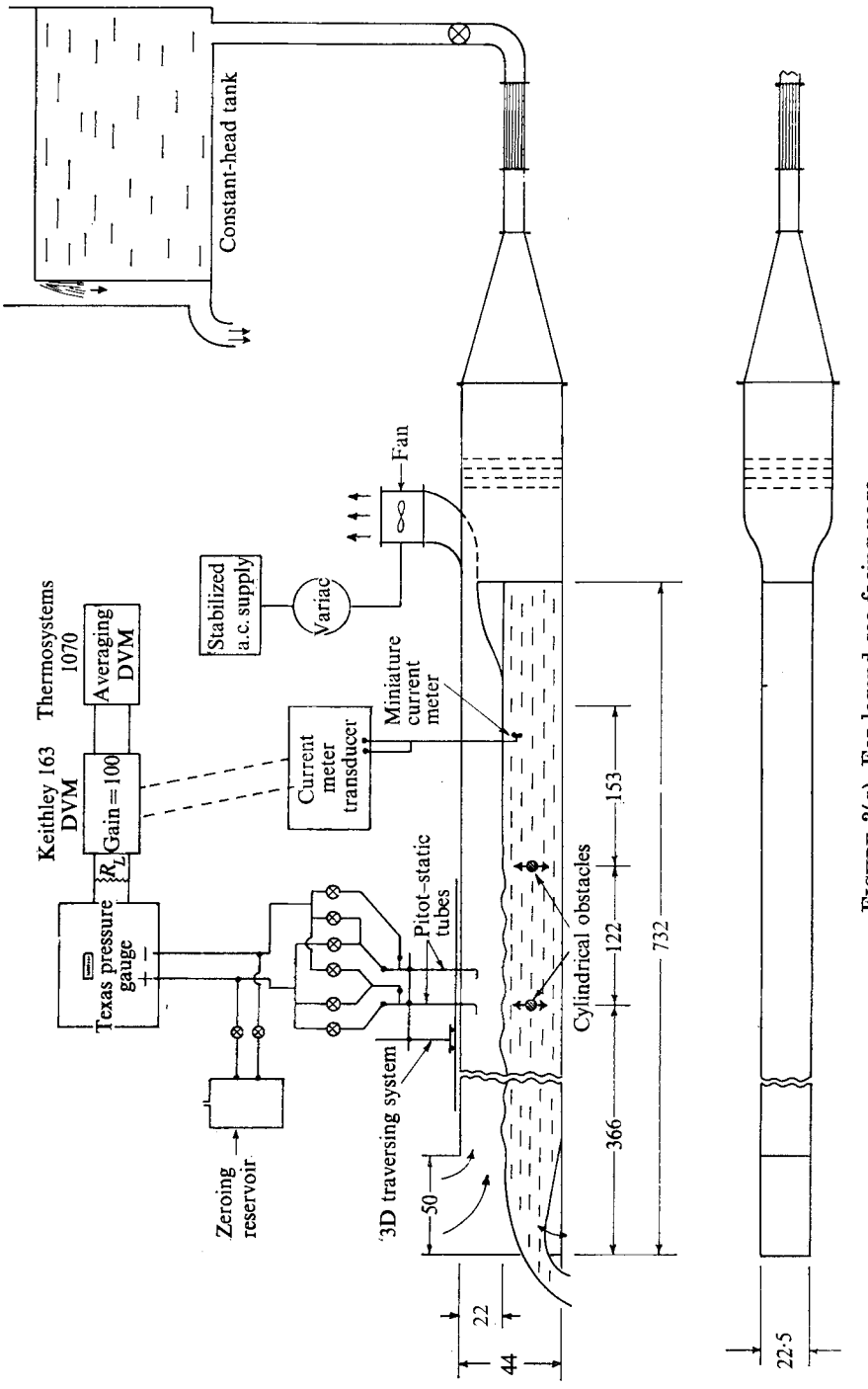


FIGURE 3(*a*). For legend see facing page.

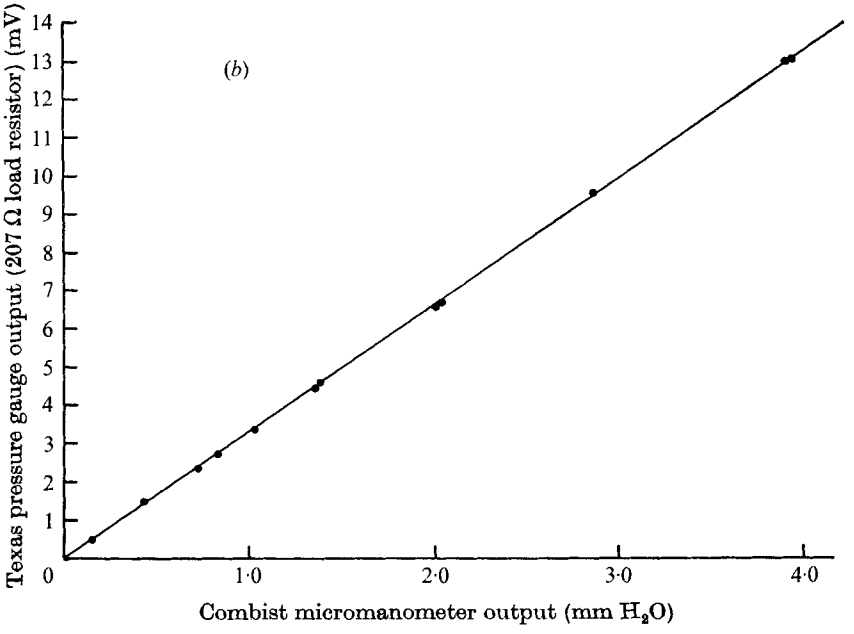


FIGURE 3. (*a*) The experimental configuration (not to scale; all dimensions in centimetres). (*b*) Calibration curve for the Texas precision pressure gauge.

downwind, adverse pressure gradient). On the basis of the discussion above we envisage a mean streamline pattern for the separated flow as shown in figure 2 (*a*) if the next downwind wave is breaking and as shown in figure 2 (*b*) if this wave is unbroken. The latter configuration is appropriate to the experiments reported in this paper.

## 3. The experimental facility

The measurements and flow-visualization studies were carried out in an open-circuit wind-wave flume, shown in figure 3 (*a*). The water flowed from a constant-head tank via a diffuser-settling chamber-contraction section to provide a smooth flow in the working section. The water level and flow speed were adjustable over a wide range by varying the inlet flow rate and downstream weir height. This arrangement provided a water flow which had excellent long-term stability, with minimal fluctuations of the free-surface level ($< 1$ mm amplitude). The curved entry plate served to damp these fluctuations, at the same time providing a suitable exit transition for the air flow. The unbroken standing wave train was produced as the water flowed over a submerged smooth cylinder (4·2 cm diameter). In all the experiments the depth of this upstream obstacle was set such that the leading wave was just short of breaking, thereby providing a train of unbroken waves of maximum attainable amplitude. For the breaking-wave studies, a second cylindrical obstacle was installed downstream of the first. It had the same diameter and could be placed at any desired depth. When it was appropriately positioned, it generated a statistically steady breaking wave immediately downstream, embedded in a train of finite amplitude but non-

breaking waves. (For a fixed obstacle separation, only those water velocities giving rise to an integral number of waves in this distance gave rise to useful configurations.)

The air was drawn over the water by a variable-speed axial-flow fan powered by a variac fed from a stabilized a.c. power supply. This provided a developing boundary-layer flow in the working section with centre-line speed capability of 0–6 m/s. During any experimental run, the air-speed stability was better than $\pm 0{\cdot}5\,\%$. The day-to-day reproducibility for a fixed fan supply voltage was also $\pm 0{\cdot}5\,\%$.

The quantitative data runs consisted of measuring profiles of static and velocity head as well as the differences in static pressure and total head over two consecutive wave crests. Two miniature (2·3 mm diameter) elliptic-nosed Pitot–static tubes (Airflow Developments) were used for all the data collection. They were mounted on a traverse system adjustable in three dimensions at a streamwise separation of 37 cm, the nominal wavelength of the waves studied. The elevations of the sensors above the mean water level were matched to better than 0·5 mm at each profile height using a cathetometer. The pressure transducer used was a Texas Instruments Precision Pressure Gauge Type 145 with a 0–5 p.s.i. (differential) capsule. Its output was amplified 100 times through a Keithley Type 163 D.V.M. and fed to a Thermo-Systems Type 1070 averaging voltmeter where 100 s time constant averages were taken. The linearity of the system was determined *in situ* using a Combist micromanometer and is shown in figure 3(*b*). The probes were connected according to the differential system shown in figure 3(*a*) in order to minimize the effects of two principal sources of error: thermally induced zero drift in the pressure gauge and small but persistent long-term oscillations in the air flow. The effect of zero drift in the system was accounted for by recording the zero after every second pressure reading. The differential connexions allowed accurate determination of the difference quantities over consecutive crests in spite of the small long-term oscillations in the air flow. With this system we could resolve pressure differences down to $3 \times 10^{-3}$ mm $H_2O$ with a repeatability of $\pm 1{\cdot}2 \times 10^{-2}$ mm $H_2O$. Prior to the data runs we checked the lateral uniformity of the mean air flow and found less than 1 % variation over a span of $\pm 3$ cm from the centre-line. We also could not detect any probe interference effects due to the wake of the upstream probe. To ensure repeatability it was necessary to monitor the upstream water speed. A miniature current meter was used and its output allowed matching the water speed to within 1 % for each data run.

The quantitative data runs were complemented with flow-visualization studies carried out at low wind speeds (centre-line velocities $U_c$ of about 0·9 m/s) where sufficient smoke density could be maintained for successful photography. The smoke source was kerosene vapour produced by a simple generator. An electronic flash provided the illumination through a 1 cm wide collimator positioned above the tunnel centre-line. Smoke was introduced continuously in close proximity to the water surface at a location downwind of the particular wave crest under study. Care was taken to ensure that the smoke possessed very little momentum of its own. In this manner sufficient smoke was convected by the air flow in

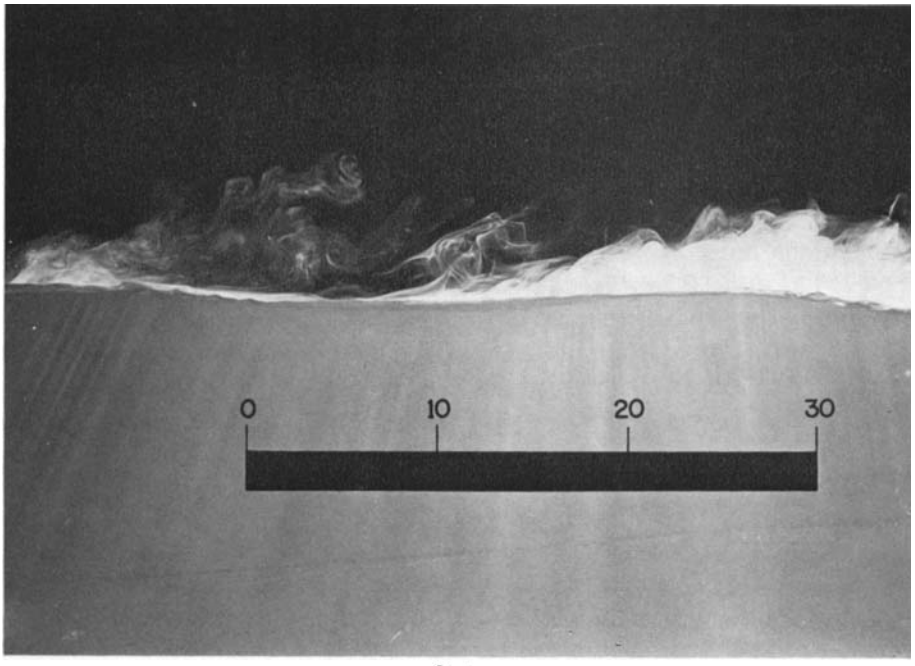


(*a*)

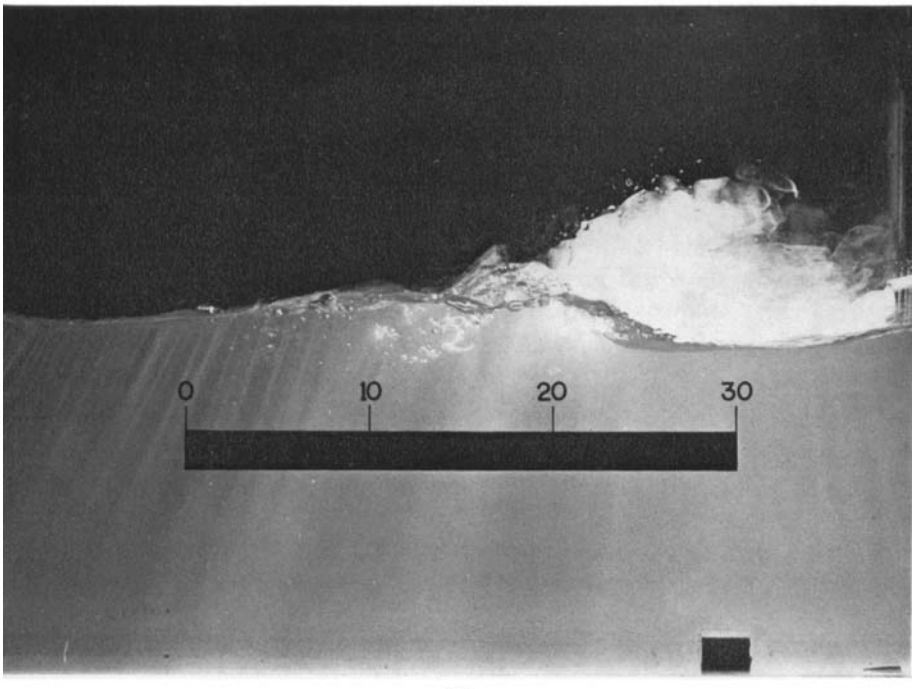


(*b*)

FIGURE 4. Smoke visualization for the air flow over (*a*) an unbroken finite amplitude water wave and (*b*) a breaking water wave. The superimposed scale is in cm. The air flow is from left to right with $U_e = 0{\cdot}9$ m/s. The water flow is from right to left at 0·75 m/s. The smoke was introduced continuously at the far right-hand side.

the vicinity of the water surface to indicate whether the flow remained attached, with the smoke passing upwind over the wave crest, or whether separation occurred, with the smoke lifting away into the free stream.

## 4. Experimental results

### *Flow-visualization studies*

The flow-visualization studies were feasible only at low wind speeds. In the photographs shown here, the centre-line wind speed was 0·9 m/s and the wavelength was nominally 37 cm. The character of the air flow over the unbroken and broken waves is depicted clearly in figures 4(*a*) and (*b*) (plate 1) respectively. In figure 4(*a*) the smoke is seen to pass over the crest of the unbroken wave and whilst much is entrained by the overlying air flow, there is still evidence of upwind smoke attachment beyond the next crest. The opposite is true for the breaking wave (figure 4*b*); here the boundary fluid is seen to lift off the wave surface at the forward stagnation point and is swept downwind, thereby creating a separation zone downwind of the breaking wave's crest. It should be pointed out that the occurrence of the separation mechanism at such low wind speeds indeed draws attention to its tendency to occur even in the lightest breeze.

### *Quantitative results*

While the flow visualization demonstrated the concomitance of air-flow separation and wave breaking, it provided neither a measure of the dynamical importance of separation nor any assurance that separation would occur at higher wind speeds. To complement these studies measurements were made at higher wind speeds to indicate the persistence of separation and its occurrence *only* over breaking waves as well as to estimate the drag over the broken and unbroken wavy surfaces. From the pressure measurements, made as described in § 3, we obtained profiles of the momentum flux differential between two successive crests for the air flow over an unbroken wave of finite amplitude ($ak \simeq 0{\cdot}2$, where $a$ and $k$ are the amplitude and wavenumber respectively) and over a breaking wave of the same nominal wavelength, both waves being embedded in a train of unbroken finite amplitude waves. A reference run over a wind-ruffled quasi-flat water surface at the same nominal wind speed and water speed was included in the data collection.

Our wind-wave flume had the usual limitations of finite fetch, air channel height and aspect ratio, so we were mainly concerned with *relative differences* in the profiles of momentum flux differential ($\Delta M = 2\Delta P_T - \Delta P_s$, where $\Delta P_T$ and $\Delta P_s$ are the measured total pressure and static pressure differentials respectively) among the three flows. Drag differences resulting from changes in the lower boundary condition were then estimated from the integrals of the profiles of momentum flux differential and effective surface shear-stress values were computed for each case.

A comprehensive data run was made for a centre-line wind speed of approximately 4·3 m/s with a confirming run at 5·9 m/s. The repeatability of both runs was investigated thoroughly and is shown by the scatter in the figures. For the

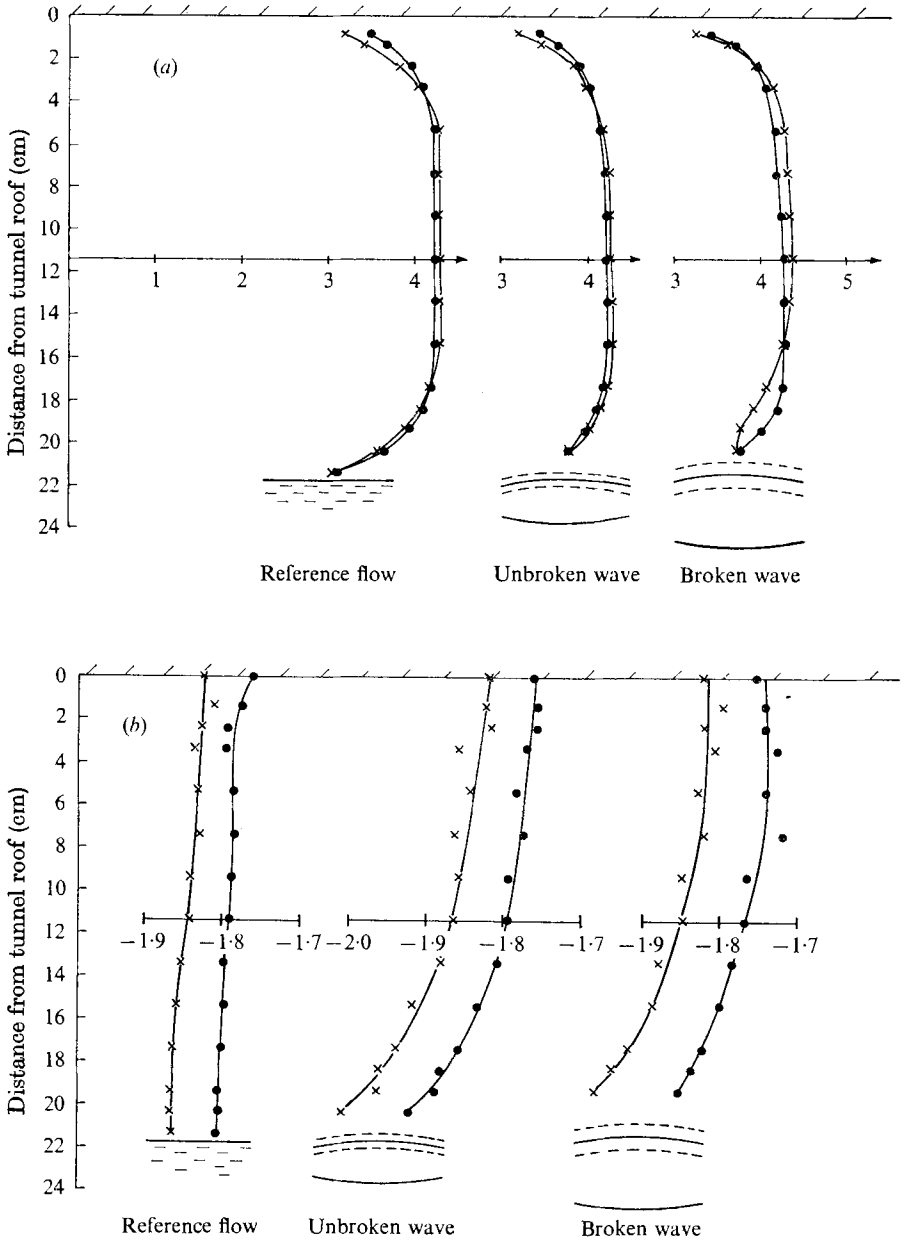


FIGURES 5(*a*, *b*). For legend see facing page.

4·3 m/s run we recorded the upstream and downstream profiles of total pressure and static pressure (relative to atmosphere) together with profiles of total pressure and static pressure differentials. For the run at the higher wind speed we omitted the downwind total and static pressure profiles, calculating them subsequently from the upstream and differential data. The results for the two wind speeds are shown in figures 5 and 6.

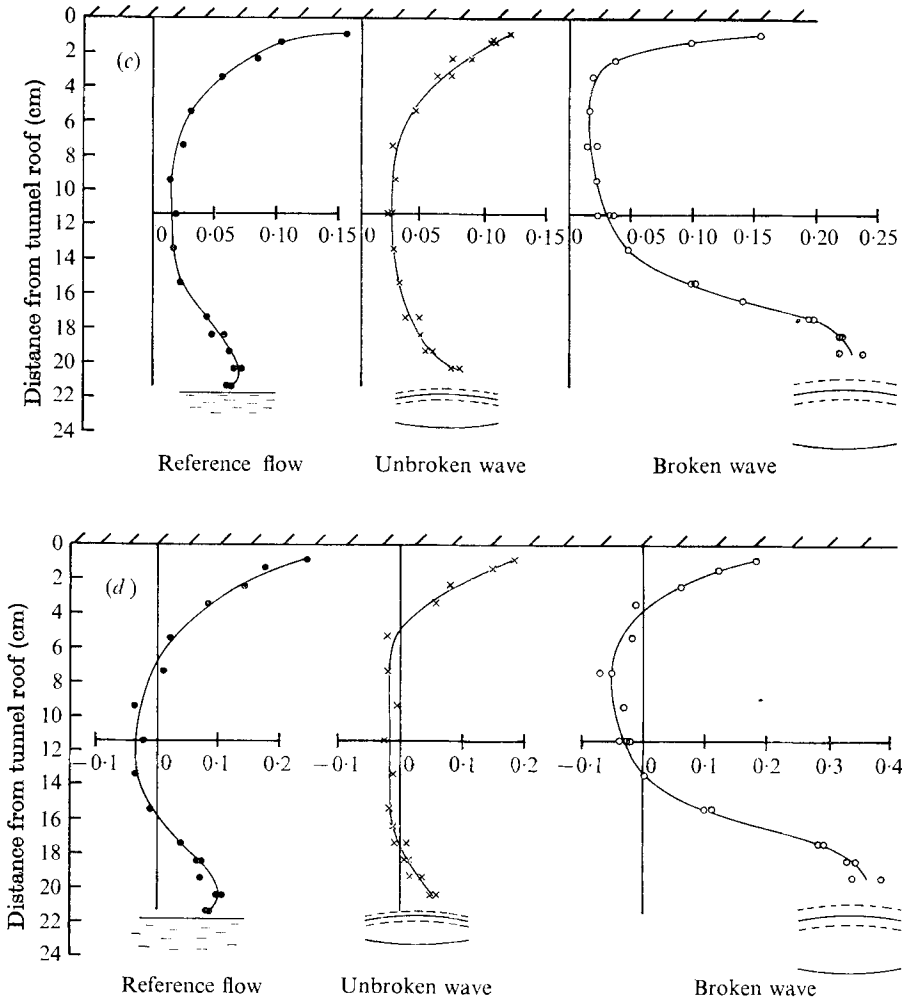


FIGURE 5. Low-speed ($U_c = 4{\cdot}3$ m/s) results. ——, mean water levels for crest and trough; – – –, level fluctuation limits. (*a*) Mean velocity profiles in m/s; •, upwind values; ×, downwind values. (*b*) Static pressure profiles relative to atmospheric in mm $H_2O$; symbols as in (*a*). (*c*) Total head differential profiles measured over a wavelength (37 cm) between successive crests in mm $H_2O$. (*d*) Momentum flux differential profiles measured over a wavelength (37 cm) between successive crests in mm $H_2O$.

The following features are evident from the results.

(i) The particularly large drag increment due to the breaking wave. This is seen to arise from a velocity wake in the downstream velocity profiles and is confirmed as a strongly dissipative region in the total-head differential profiles. This strongly indicates the existence of separated air flow over the broken wave. Actual values of the measured drag are given below.

(ii) The momentum deficit or drag measured for the unbroken wave was an order of magnitude lower, evidently below that of the wind-ruffled quasi-flat flow. This effect, somewhat unexpected initially, is examined in the discussion

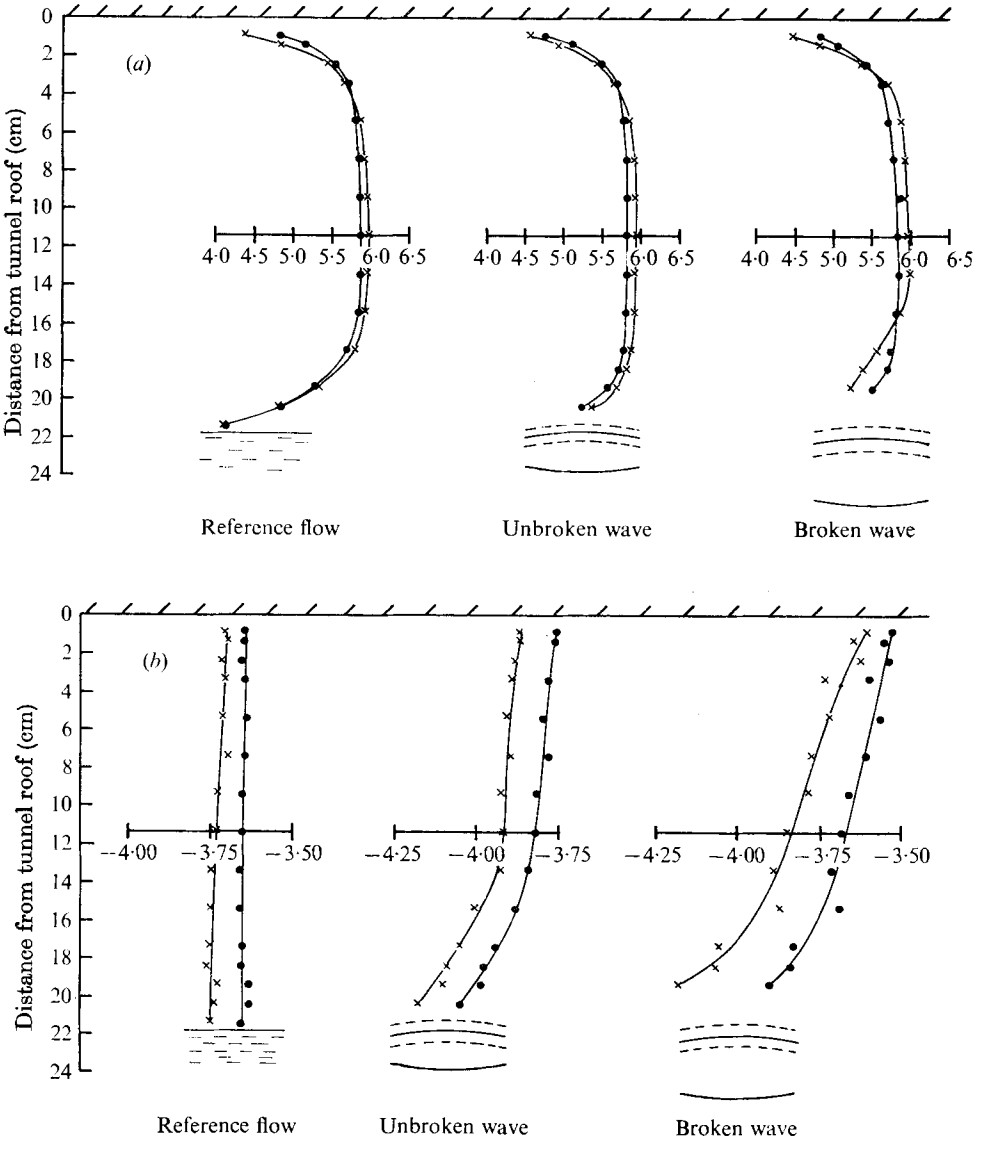


FIGURES 6 (*a*, *b*). For legend see facing page.

(§ 5). For the unbroken wave, the velocity, pressure, total head and static head differentials all serve to indicate the approximate recovery of the air flow from one crest to the next apart from the effects of the developing free stream. This supports the assertion that the air flow did not separate over unbroken waves, even at the highest wind speeds in this study.

It is felt that the results expressed in (i) and (ii) offer strong confirmation that air-flow separation occurs for wind co-flowing over water waves if and only if the waves are breaking. It is further evident that breaking waves give rise to far larger effective shear stresses at the water surface.

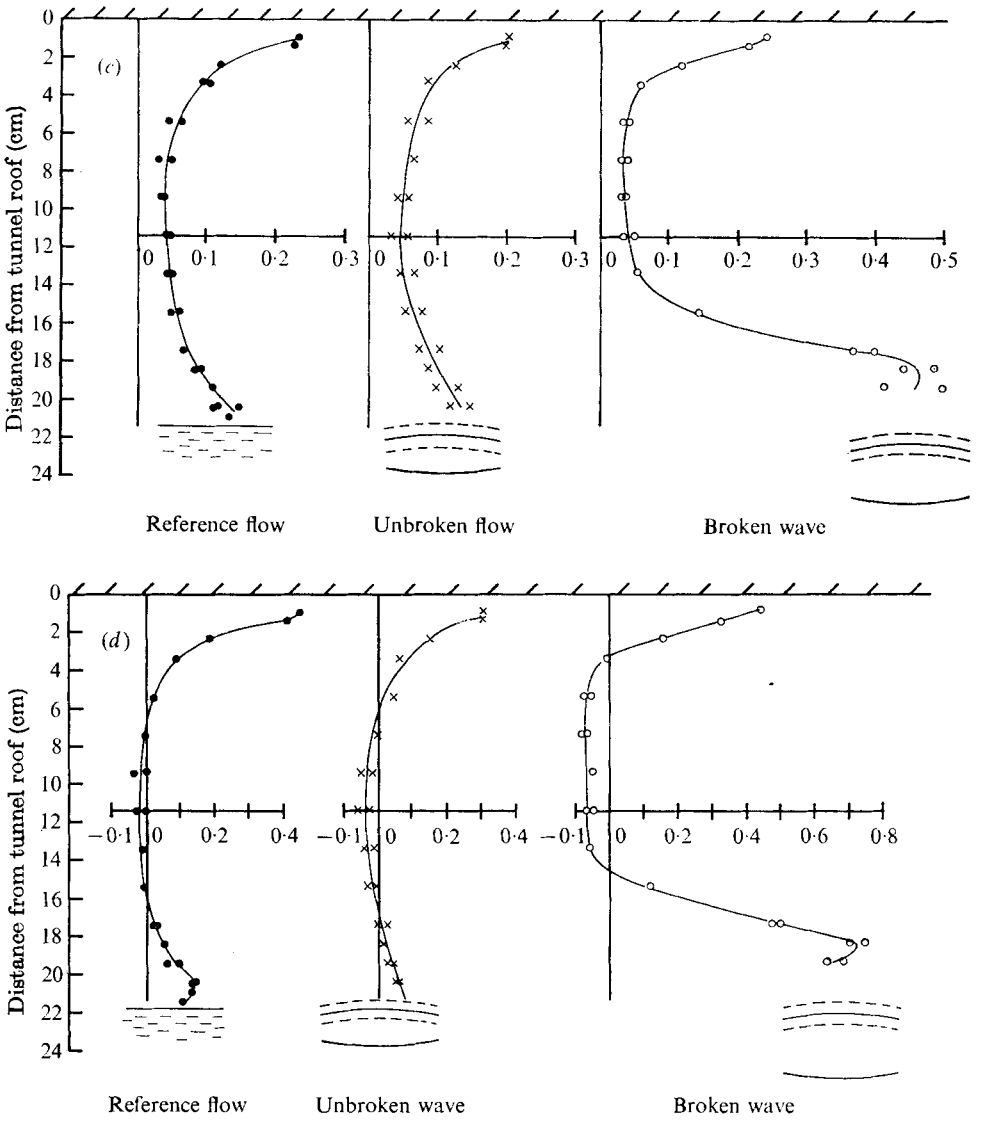


FIGURES 6(*a*, *b*). High-speed ($U_c$ = 5·9 m/s) results. The notation is exactly as for figure 5.

The experimental facility was not ideally suited to an absolute determination of the momentum flux across the interface. However, we have estimated the drag as follows. The momentum budget was estimated in a two-dimensional control volume bounded by the lower surface, the upstream and downstream stations and a plane surface in the central uniform-flow region 10 cm from the channel roof. The mass and momentum fluxes across this latter surface were assumed to be zero. Because of fluctuations of the lower boundary we were unable to measure the streamwise momentum flux deficit in the lowest centimetre of the air channel. This required extrapolating the profiles to the water surface, a

| Wind speed (m/s) | Surface shear stress (dynes cm$^{-2}$) Wind-ruffled surface | Unbroken wave | Broken wave |
|---|---|---|---|
| 4·3 | 0·7 | 0·1 | 4·9 |
| 5·9 | 1·1 | 0·2 | 8·8 |

TABLE 1. Mean interfacial shear stresses estimated from momentum flux deficit profiles in figures 5(*d*) and 6(*d*)

procedure which is likely to be least accurate for the unbroken wave: the other configurations displayed evidence of their momentum flux deficits reaching maxima above the interface while the profiles for the unbroken waves were still increasing monotonically at the measuring station closest to the interface. Another source of error arose from the convergence effect due to the downwind growth of each side-wall boundary layer. No measurements were made to assess this effect, but it is likely to have been of the same order of magnitude as that due to the roof boundary layer. As can be seen from the figures, in the free stream such convergence gives rise to flow acceleration, which appears as a negative momentum flux in the central region of the flow; the effect of this convergence on the flow near the air–water interface is less certain. If it were assumed that this convergence effect was uniform over the control volume's depth, this would imply that our measured stress values would tend to underestimate the actual values. Finally, we did not correct our Pitot-tube measurements for effects of the turbulence level, which were believed to be small. On these grounds we do not claim a high level of precision in the reported stress values. On the other hand, owing to the relative nature of the experimental configuration, it is felt that the large differences observed for the air flow over unbroken and broken waves can leave little doubt as to the strong dissimilarities, both qualitative and quantitative, between the two flows.

With these qualifications we estimated the shear stress by dividing the integrated momentum flux deficit by the wavelength. The results are given in table 1. On the basis of the uncertainties described above, we estimate that variations of up to $\pm 25\,\%$ are possible in the quoted stress values.

## 5. Discussion

The primary aim of this paper has been to establish that, when wind blows over surface gravity water waves, the air flow will not separate *unless* wave breaking is occurring, in which case separation occurs ahead of each breaking wave's crest. Our wave flume experiments consistently supported this assertion over the important short gravity wave range (10–37 cm wavelength) for centreline wind speeds up to 5·9 m/s (the upper limit for a stable stationary wave profile in the flume). In addition, the pressure measurements served to point out the following.

(*a*) The serious modification to the pressure and velocity distributions in the air flow over a breaking wave. In this wind-wave flume study, these effects were evident at elevations of several times the wave amplitude above the mean water level. In an unconfined flow similar effects should be seen.

(*b*) The particularly large increment in drag over a breaking wave compared with that over a finite amplitude unbroken wave of the same nominal wavelength when each wave was embedded in a train of finite amplitude unbroken waves. Under these conditions, our results show a drag augmentation of 49 times at $U_c = 4{\cdot}3$ m/s and 44 times at $U_c = 5{\cdot}9$ m/s.

In attempting to extrapolate our wave flume results to the oceanic situation it is apparent that certain intrinsic scalings might not be well matched. In particular, the heights of the logarithmic region clearly differ. However, we shall tentatively assume a logarithmic extrapolation of our velocities at $z = 10$ cm to $z = 10$ m and check the resultant scalings *a posteriori*. Centre-line wind speeds of 4·3 and 5·9 m/s for the quasi-stationary 37 cm wave correspond to air speeds of 5·03 and 6·63 m/s for propagating 37 cm waves. The logarithmic conversion to the height 10 m yields $U_{10} = 15{\cdot}1$ m/s and $U_{10} = 19{\cdot}9$ m/s respectively. Thus for our given wavelength ($\lambda = 37$ cm) the Reynolds number $U_{10}\lambda/\nu_a \sim 7 \times 10^6$, a value not atypical for short gravity waves in the ocean. Further, the usual correlation for the average wind stress over the ocean $\tau_s = \rho_a C_D U_{10}^2$ with $C_D = 1{\cdot}3 \times 10^{-3}$ (Stewart 1974) yields values of 3·6 dynes cm$^{-2}$ and 6·1 dynes cm$^{-2}$ at these two effective wind speeds. These shear stresses are considerably higher than those which we measured for the wind-ruffled and unbroken wave surfaces, but somewhat smaller than those measured for the broken wave. This suggests strongly that the drag coefficient of the air–sea interface is too large to be accounted for solely by the momentum transfer across an unbroken wavy surface. The presence of intermittent breaking appears to be necessary to account for the field measurements. The above stress comparisons suggest that the shear velocity ($u_*$) correspondence is reasonable.

Finally we consider the roughness-height ($z_0$) scaling. For the ocean $z_0$ lies typically in the range 1–10 cm for $10 < U_{10} < 20$ m/s. Our cases of a wind-ruffled flat surface and unbroken waves had $z_0$ values between 0·01 mm and 1 mm but for the broken wave, although difficult to assess directly from our results, it is not unlikely that the effective roughness height would be much closer to the ocean values in view of the relatively large perturbation the breaking wave induces in the air flow near the interface.

Other important effects become apparent in a comparison between our results for the drag over unbroken waves and over a wind-ruffled quasi-flat water surface. Two noteworthy features are immediately evident. First, the unbroken wave induces *less* drag than the wind-ruffled surface. This appears to arise from the suppression of the small wind-wavelets by the combined effects of wind drift and the underlying larger-scale wave motion, an effect investigated in II. Second, it was observed that the drag over the water surface for these two cases was somewhat less than that due to the roof boundary layers. Although precautions were taken, we cannot be absolutely certain that the segmented roof was either ideally smooth or completely air-tight, which might have contributed

to increasing the drag there, even though the results were repeatable over a time separation of a week during which the roof segments were moved frequently. In addition, the asymmetric air-channel inlet configuration may account for some of the differences. So we must defer any conclusions concerning a comparison with flat-plate values.

As pointed out in § 1, there has been much speculation on the question of the occurrence of air-flow separation over wind waves but little direct evidence has been forthcoming from earlier theory or observation. Our results will now be compared with some recent studies in which this question has been considered.

Chang *et al.* (1971) made comprehensive measurements in the air flow over equilibrium wind waves with a dominant frequency of 2·4 Hz in their large wind-wave facility. Their free-stream wind speeds were nominally 7·7 m/s and 9·8 m/s, giving $c/u_* \sim 1$. By using an electromechanical wave follower, they could maintain their sensor at a fixed height above the instantaneous water surface. From their results, they concluded that the air flow did separate over their dominant wind waves. Since their equilibrium waves were necessarily breaking intermittently, their observations are consistent with our air-flow separation criterion.

Wu (1969) formulated a somewhat different criterion for air-flow separation, based on certain physical arguments and indirect experimental evidence. He proposed that separation occurs over waves with phase velocities less than the shear velocity. Our results neither confirm nor refute this criterion directly. However, Wu correlates a basic change in the measured roughness height $z_0$ with the onset of wave breaking for the dominant wind waves in his laboratory wind-wave tank. He suggests that air-flow separation might be expected and would account for the rapid change in surface roughness. Therefore his observations also support our separation criterion.

From the results of this study, it is evident that further work is needed on the effects of breaking waves on the air flow above the sea surface. Of particular interest is the role of wind-generated small-scale breaking waves distributed over an underlying large-scale wave motion. This problem has been studied recently by Longuet-Higgins (1969*b*) and Hasselmann (1971). Longuet-Higgins (1969*b*, p. 373) envisaged a maser mechanism based on the "sweeping up of short wave momentum by long waves". Hasselmann (1971, p. 198) explicitly assumed that "the momentum transfer $T_\alpha^a$ from the atmosphere is not modulated by the long waves". In effect, therefore, both authors have examined the coupling between the wind field and sea surface on the basis that the wind stress serves *only* to supply momentum to the small-scale wave field, which in turn is considered as the sole source of momentum available to the large-scale wave field. Longuet-Higgins concluded that the energy transfer according to this process was significant while Hasselmann came to the opposite conclusion.

The work reported here suggests a clarification of the role of the small-scale breaking waves. While their dynamics may be of little direct significance in energizing the large-scale wave field, their kinematic effect of creating a distribution of localized pockets of separated air flow, moving relative to the large-

scale wave field, appears to be significant dynamically both in wind-wave generation and in driving surface currents. In this context, we envisage the following: Phillips (1966, § 3.7, p. 61) has described the mechanisms which result in the shortening and steepening of short waves riding over the crests of longer waves, with the opposite occurring in the troughs of the long waves. Notwithstanding any additional effects imposed by the wind-drift layer or by local pressure gradients in the air flow, it is not unreasonable to expect a strong correlation between the distribution of shear stress induced by the small-scale breaking waves and the long-wave elevation. As was previously pointed out by Longuet-Higgins (1969*a*, *b*), this would constitute an effective momentum flux to the long waves for the case where the long waves and wind are travelling in the same direction and a momentum flux from the long waves for the counter-flow situation. These cases correspond to long-wave growth and damping respectively. Further, the effective stress due to the distribution of breaking wavelets must possess a positive mean value when averaged over the long-wave ensemble. This component would then correspond to a mean stress driving the surface current. The above hypothesis is in effect a revision of the maser mechanism proposed by Longuet-Higgins (1969*b*). In the original hypothesis, the virtual stress arose from the short-wave momentum; here the virtual stress arises externally from the air flow separating locally over small-scale breaking waves.

It is clear that the above hypothesis is speculative but it is felt that the results of this study offer encouragement to its further investigation.

The authors gratefully acknowledge the co-operation and assistance of their colleagues at the Water Research Laboratory, Manly Vale, where the experiments were conducted. They also wish to thank B. Motson and N. Pitsis for their generous loan of equipment. This research was supported by the Australian Research Grants Committee.

## REFERENCES

BANNER, M. L. & PHILLIPS, O. M. 1974 *J. Fluid Mech.* **65**, 647.

BARGER, W. R., GARRETT, W. D., MOLLO-CHRISTENSEN, E. L. & RUGGLES, K. W. 1970 *J. Appl. Met.* **9**, 396.

BARNETT, T. P. & KENYON, K. E. 1975 *Rep. Prog. Phys.* **38**, 667.

BATCHELOR, G. K. 1967 *An Introduction to Fluid Dynamics.* Cambridge University Press.

CHANG, P. C., PLATE, E. J. & HIDY, G. M. 1971 *J. Fluid Mech.* **47**, 183.

HASSELMANN, K. 1971 *J. Fluid Mech.* **50**, 189.

JEFFREYS, H. 1924 *Proc. Roy. Soc.* A **107**, 189.

JEFFREYS, H. 1925 *Proc. Roy. Soc.* A **110**, 341.

KENDALL, J. M. 1970 *J. Fluid Mech.* **41**, 259.

LONGUET-HIGGINS, M. S. 1960 *J. Fluid Mech.* **8**, 293.

LONGUET-HIGGINS, M. S. 1969*a* *Phys. Fluids*, **12**, 737.

LONGUET-HIGGINS, M. S. 1969*b* *Proc. Roy. Soc.* A **311**, 371.

MOTZFELD, H. 1937 *Z. angew. Math. Mech.* **17**, 193.

PHILLIPS, O. M. 1966 *The Dynamics of the Upper Ocean.* Cambridge University Press.

PHILLIPS, O. M. & BANNER, M. L. 1974 *J. Fluid Mech.* **66**, 625.

STANTON, T. E., MARSHALL, D. & HOUGHTON, R. 1932 *Proc. Roy. Soc.* A **137**, 282.

STEWART, R. W. 1974 *Boundary-Layer Met.* **6**, 151.

URSELL, F. 1956 In *Surveys in Mechanics* (ed. G. K. Batchelor), p. 216. Cambridge University Press.

WU, J. 1969 *Tellus*, **21**, 707.